Catalysis Science & Technology

Accepted Manuscript

This is an *Accepted Manuscript*, which has been through the Royal Society of Chemistry peer review process and has been accepted for publication.

Accepted Manuscripts are published online shortly after acceptance, before technical editing, formatting and proof reading. Using this free service, authors can make their results available to the community, in citable form, before we publish the edited article. We will replace this *Accepted Manuscript* with the edited and formatted *Advance Article* as soon as it is available.

You can find more information about *Accepted Manuscripts* in the Information for Authors.

Please note that technical editing may introduce minor changes to the text and/or graphics, which may alter content. The journal's standard Terms & Conditions and the Ethical guidelines still apply. In no event shall the Royal Society of Chemistry be held responsible for any errors or omissions in this *Accepted Manuscript* or any consequences arising from the use of any information it contains.

ROYAL SOCIETY OF CHEMISTRY

www.rsc.org/catalysis

Cite this: DOI: 10.1039/c0xx00000x

www.rsc.org/xxxxxx

ARTICLE TYPE

Simultaneous tetralin HDA and dibenzothiophene HDS reactions on Ni-Mo bulk sulphide catalysts obtained from mixed oxides

Yordy E. Licea,[a] Sandra L. Amaya,[b] Adriana Echavarría,[b] Jefferson Bettini,[c] Jean G. Eon,[a] Luz A. Palacio[d] and Arnaldo C. Faro Jr.*[a]

Received (in XXX, XXX) Xth XXXXXXXXX 20XX, Accepted Xth XXXXXXXXX 20XX
DOI: 10.1039/b000000x

Ni-Mo bulk sulphide catalysts were obtained from mixed-oxides. The mixed-oxides were obtained by calcining a -synthesized lamellar precursor with the so-called ϕ_y structure and formula $(NH_4)H_{2x}Ni_{3-x}(OH)_2(MoO_4)_2$. The corresponding mixed-oxides obtained by calcination were characterized by nitrogen adsorption, XRD, and ICP. Mixtures of α-$NiMoO_4$ and β-$NiMoO_4$ were obtained. A batch reactor was used for CS_2/n-hexadecane *in situ* sulphidation of the mixed-oxides. A mixture of dibenzotiophene and tetralin was used for liquid phase reaction carried-out at 613 K and 70 bar. After the catalytic tests, the bulk sulphide catalysts were characterised by nitrogen physical adsorption, synchrotron-light XRD, EXAFS and HR-TEM. The EXAFS simulations are consistent with disordered nickel sulphide particles dispersed in the catalysts. HR-TEM images showed randomly oriented, stacked-layer particles typical of Mo sulphide. The bulk catalysts had larger HDS and HDA activities and selectivities for hydrogenation reactions than an alumina supported conventional catalysts containing the same Ni:Mo ratio. A pronounced support effect was observed for both HDS and HDA reactions. The use of the support strongly suppressed both cyclohexylbenzene formation in HDS of DBT and cis-decalin formation in HDA of tetralin. This suggests that similar active sites are involved in the formation of these compounds on one hand, while another type of site is involved in biphenyl and trans-decalin formation on the other.

1 Introduction

Sulphur environmental restrictions have been strongly tightened in the last 20 years in several countries [1] and ultra-low sulphur diesel (ULSD) has been targeted by refineries as a consequence [2]. Hydrotreating is the main process responsible for the quality of transportation fuels in refineries and, besides sulphur removal from organo-sulphur molecules in the diesel (HDS: hydrodesul phurization), nitrogen removal (HDN: hydrodenitrogenation) and hydrogenation of aromatics (HDA: hydrodearomatisation) also occur in the presence of hydrogen.

The development and fundamental understanding of catalysts used in hydrotreating processes have been the subjects of many studies for more than four decades, and sulphided Ni(Co)-Mo(W) alumina-supported catalysts are the most widely used in the industry [3]. Recently, unsupported sulphides of the same metals have been claimed to have a strong hydrogenating power [4]. This is supposed to render the hydrotreating process more efficient in removing sulphur from the most refractory molecules in diesel, *via* the hydrogenation pathway [5]. A high hydrogenation activity is also desirable for the HDA reaction, which is important for obtaining diesel fuels with higher cetane number and lower polyaromatic hydrocarbon contents, properties which are also specified in recent legislation [6-8].

Several studies with unsupported catalysts obtained from organic thiosalts or organo-metallic compounds have appeared in the open literature [9-12], but this sort of preparation method is difficult to implement in practice, due to the costs involved and the use of toxic ammonium sulphide or hydrogen sulphide bubbling in the preparation of the precursors, as pointed-out in the literature [13, 14]. Few papers concerning their synthesis from metals mixed oxides have appeared since unsupported sulphides were patented. A precursor Ni-Mo-W ammonium compounds (synthesized according to an Exxon Mobil patent [15]) has been sulphided by Gochi et al. [16] using different agents and the resulting materials were tested as catalysts in the HDS of dibenzothiophene (DBT). The precursor salt was sulphided without previous calcination. A relation between the HDS activity of the catalysts and their textural properties -determined by the sulphiding agents- was claimed by the authors [16].

Wang et al.[17] have also synthesised Ni-Mo-W precursors using lab-synthesised or commercial nickel carbonate. The precursors were sulphided without previous calcination, and the materials so obtained were tested in the HDS of 4,6-dimethyl-dibenzothiophene. The higher HDS activity values for the synthesised catalysts was attributed to the better contact between the $Mo(W)S_2$ particles and the Ni_7S_6 slabs, which, according to the authors, should increase the Ni-Mo(W)-S sites formation.

In the present work, bulk NiMo catalysts were obtained from sulphidation of a NiMo mixed oxide. The mixed oxide was previously obtained by calcination of a layered precursor with

Catalysis Science & Technology Accepted Manuscript

nominal formula $(NH_4)H_{2x}Ni_{3-x}(OH)_2(MoO_4)_2$ (with $0 \le x \le 3/2$) whose crystal structure was resolved by Levin et al. [18] and belongs to a family of phases with general formula $NH_4(M_{II})_{3-x}H_{2x}(OH)_2(MoO_4)_2$, where M_{II} is a divalent cation (Co^{2+}, Ni^{2+}, Cu^{2+}, Zn^{2+}), originally reported by Pezerat [19] and denominated ϕ_y phases. Briefly, these layered phases consist of MoO_4 tetrahedra linked with $M_{II}O_6$ octahedra to form negatively charged layers. The negative charge is compensated by protons associated with the basal plane of the layers and ammonium ions in the interlayer space. The attractiveness of these materials as possible catalyst precursors lies in the fact that the active components (Ni and Mo in our case) are completely mixed at the atomic level and also that gaseous substances are produced upon calcination (ammonia and steam), which may be expected to generate porosity in the calcined material. The use of catalysts derived from these materials in selective oxidation reactions has been reported [20].

Most model compound studies reported for unsupported catalysts involve only the HDS reaction (DBT or/and 4,6-dimethyldibenzothiophene [14, 21-26]) but, as mentioned earlier, there is currently much interest in the HDA function of hydrotreating catalysts [27]. Results with real feeds are reported in the literature [28-31], but these are difficult to interpret from a molecular standpoint.

In this work, the catalysts were characterised by several physicochemical techniques and their activity and selectivity in the sulphided state were evaluated in the simultaneous HDS of dibenzothiophene (DBT) and HDA of tetralin (tetrahydronaphtalene, THN), the results being compared with those obtained with conventional alumina-supported NiMo catalysts. An interpretation is attempted for the striking differences in selectivity observed between the supported and the unsupported sulphides, not only in the HDS of DBT, but also in tetralin hydrogenation.

2 Experimental

2.1. Synthesis

Two layered NiMo precursors were synthesised by a co-precipitation method. Nickel nitrate (or sulphate) and ammonium heptamolybdate aqueous solutions were prepared each containing quantities of Ni and Mo to obtain an equimolar Ni:Mo solution after the Ni solution was added to the Mo one. By the slow addition of NH_4OH, the pH of the solution was increased to about 8. The solution was then transferred to a closed bottle, where a treatment was carried-out for 4 hours at 353 K. The green precipitate obtained was then washed with water to reach neutral pH and then dried for 24 hours. The synthesised materials using nickel nitrate or nickel sulphate were named NH_4-NiMo-a and NH_4-NiMo-b, respectively.

In order to obtain the mixed-oxides, the solids were heated under static air at 5 K min^{-1} heating rate to 673 K and maintained at this temperature for 3 h. The calcined materials were named NiMo-a-ca and NiMo-b-ca. The calcination temperature was chosen with basis on thermogravimetric analysis of the precursors, to be above the decomposition temperature of the ϕ_y phase, established from the weight loss due to ammonia and water evolution, and to maximise the surface areas of the calcined precursors.

The sulphidation was performed *in-situ*, immediately before the catalytic tests, as described under 2.7, and the sulphide catalysts were named NiMo-as and NiMo-bs. An alumina supported NiMo material synthesised in our laboratory [32] and a commercial alumina supported NiMo catalyst containing phosphorous were also evaluated.

2.2. Elemental analysis

Quantitative analysis for the metals was performed by ICP-OES in a Spectro Arcos optical spectrometer. The samples were dissolved with hot concentrated nitric acid.

2.3. X-Ray diffraction

X-ray powder diffraction (XRD) patterns for the layered precursors and mixed oxides were obtained in a Rigaku Ultima IV apparatus using CuK_α radiation (λ=0.15418 nm), operated at 40 kV and 20 mA. Scans were performed at 2º min^{-1} in the 3º to 70º range in steps of 0.02º.

The NiMo sulfide high-resolution synchrotron XRD data were collected at the X-ray powder diffraction (D10B - XPD) beamline of the Brazilian Synchrotron Light Laboratory LNLS (Campinas, Brazil), using X-rays with λ=0.12399 nm. Details of the D10B-XPD line set up may be found elsewhere [33].

Sulphided catalysts were analysed after the catalytic tests. The samples were kept under the reaction mixture itself until shortly before the XRD measurements, when they were washed first with toluene, then with n-decane in order to remove the residues from the reaction mixture. The solid soaked with n-decane was loaded into a 1 mm deep, 7 mm wide copper sample holder. A cell provided with Kapton windows was employed to slowly evacuate the solvent used to avoid sample oxidation. Several quick scans were made to test for solvent removal until the final scan was taken. The data was recorded at room temperature for 2 s/step, in steps of 0.02º from 5 to 70º (2θ).

2.4. XAS measurements

X-ray absorption spectra at Ni K-edge were taken at XAFS1 beamline at the Brazilian Synchrotron Light Laboratory, Campinas, Brazil, operated at 1.37 GeV with a maximum beam current of 250 mA. Monochromatisation of the incident beam was done using a double Si (0 0 1) crystal. The intensities of the incident and transmitted beams were monitored by Ar-filled ionization chambers. The analyses were carried-out in the ranges from 8230-9600 eV and 19900-21300 eV for Ni-K and Mo-K edges acquisition, respectively. A metal nickel or molybdenum foil was used for energy calibration reference in the respective case. The EXAFS spectra were analysed by standard procedures of data reduction using the IFEFFIT code [34]. Structural parameters were obtained from least squares fitting in R space, using theoretical phase and amplitude functions obtained from the FEFF8.2 program [35]. The parameters optimised by the software were defined as usual [36].

The analyses were performed with the catalysts in the sulphided state after the catalytic tests. The fine powders soaked in the liquids as extracted from the reactor were washed with toluene. A portion was then weighted and mixed with isopropyl alcohol for ultrasonication before the membrane was made. Kapton tape was used to cover the membrane.

2.5. Textural properties

Catalysis Science & Technology Accepted Manuscript

This journal is © The Royal Society of Chemistry [year]

A Micromeritics ASAP 2010 C equipment was used in the textural characterisation of both the calcined and the sulphided materials using nitrogen physisorption. Both the calcined and the sulphided samples were pretreated in-situ at 473 K under vacuum before the analyses. Surface areas were determined using the BET method and pore size distributions were obtained using the BJH method [37] from the adsorption branch of the isotherms.

The sulphided catalysts were analysed after the catalytic tests. The samples soaked with the reaction mixture were washed first with toluene, then with n-hexane. While soaked in n-hexane, they were placed in a Schlenk flask and heated under a N_2 flow (30 cm^3/min) for 4 h at 573 K in order to eliminate the solvent. Under the same flow, the samples were cooled down to room temperature and then the nitrogen flow was switched to a 0.5% O_2/N_2 (~80 cm^3 min^{-1}) gas mixture during 4h for surface passivation. The powder was then transferred to the ASAP sample cell, where it was heated under vacuum at 473 K and then analysed.

2.6 Electron Microscopy

A model JSM-6701F field emission scanning electron microscope (FESEM), located at Pontificia Universidade Católica do Rio de Janeiro, was used for characterising particle morphology of the NiMo-a unsupported materials at all preparation stages (layered precursor, mixed-oxide and mixed-sulphide). The precursors and the calcined oxides were placed in the sample holder without any previous treatment. Toluene and then n-hexane were employed in the washing of sulphides before placing them into the sample holder.

A JEOL model 3010 high-resolution transmission electron microscope (HR-TEM), located at the Brazilian Nanotechnology National Laboratory, Campinas, São Paulo, was used for high-resolution image acquisition of sulphide samples. It is a 300kV microscope with 1.7 Å point resolution, provided with a LaB_6 filament and an ultra high resolution pole piece. Also, it has a digital camera for images acquisition with 1024 x 1024 pixels resolution. The catalyst samples were first washed and then ultrasonicated in ethanol before some drops were placed onto a carbon-coated copper grid.

2.7. Catalytic tests

The calcined mixed-oxides were sulphided *in-situ* in a CS_2/n-hexadecane mixture in a batch Parr reactor. A careful sulphidation procedure was used, in order to avoid catalyst reduction before or after sulphidation. First, 1 g catalyst was dried under nitrogen flow at 393 K for 2 h. A 200 cm^3 amount of a 5 vol % solution of carbon disulphide in n-hexadecane was added to the reactor. The amount of CS_2 added was calculated to be 5x the stoichiometric one required to completely sulphide the unsupported mixed oxides. The same catalyst and CS_2 amounts were used in the sulphidation of the supported catalysts, despite their lower metal loading. Next, under constant stirring at 400 rpm, the reactor was pressurised to 40 bar with hydrogen, heated to 503 K under constant pressure and kept at this temperature for 2h. It was then heated to 613 K under constant pressure and kept at this temperature for 16 h. Finally, it was cooled to 593 K and vented to atmospheric pressure, in order to remove the water and hydrogen sulphide formed during the sulphidation. Our XAFS data to be discussed subsequently showed that this protocol led to essentially complete sulphidation of the catalysts. Once the sulphidation stage was finished, 5.75 g of DBT dissolved in 30 cm^3 of THN were added to the reactor. These amounts correspond to 280 ppmwt sulphur and 13 vol % THN in the reactor feed. Catalytic test conditions were then established (70 bar, 613 K, 600 rpm) and products evolution was followed by sampling small volumes of the reaction mixture for 6 h. Quantitative analysis of the reaction products was carried-out by gas chromatography in an Agilent 6890 instrument. The same chromatographic method and column (Agilent methylsiloxane 100 m X 250 µm X 0.50 µm) were used for identification of the products in an Agilent 6890 gas chromatograph equipped with a 5973A quadrupole mass selective detector.

The initial rates of conversion, R_0, for each reactant were determined from the slopes of percent conversion vs. time curves at time equals zero. Specific initial reaction rates, r_0 expressed in mol s^{-1} g_{cat}^{-1} were determined using the relation:

$$r_0 = \frac{R_0 n_0}{100 m_{cat}} \qquad (1)$$

where n_o and m_{cat} are the initial amount of reactant in the system and the catalyst mass, respectively. Additional tests were performed with the NiMo-bs catalyst: (i) a catalytic test with no DBT, to evaluate the inhibition by DBT of THN HDA, in which thiophene was added to THN (127 ppmwt sulphur) in order to maintain the catalyst in the sulphided state and (ii) a run in which the same volume of tetralin was replaced by toluene, in order to evaluate the influence of the aromatic hydrocarbon on the HDS of DBT. In the conditions used for the catalytic test, toluene does not undergo hydrogenation in the presence of DBT [38].

3 Results

3.1. Catalysis characterisation

We will first present the results for the characterisation by several methods of the unsupported NiMo catalysts prepared according to the method described under section 2.1, at all stages of their preparation, in order to have their physico-chemical properties well described. For the sulphided catalysts, a comparison is made with the sulphided supported catalyst.

3.1.1. Chemical Analyses and X-Ray Diffraction. Analysis by plasma emission spectrometry gave Ni:Mo atomic ratios of 1.64 and 1.58 for NH_4-NiMo-a and -b, respectively. These values are considerably above the 1:1 ratio used in catalysts preparation.

The XRD patterns for the layered precursors NH_4-NiMo-a and -b are presented in Fig. S1, available in the supplementary material. These patterns are typical of the NiMo layered phase described by Levin et al.[18] (ICSD-165342), with fair crystallinity. The Ni:Mo ratios obtained for these materials are slightly higher than the upper limit specified by Levin et al.[18] (1.5) for ϕ_y phases. No peaks attributable to any other Ni-containing phase could be observed in the XRD profiles.

After the precursors were calcined, mixtures of α-nickel molybdate (ICSD-81059) and β-nickel molybdate[39] were obtained, as shown in Fig. S2 in the supplementary material, but in different proportions in each case: the β phase, in which

Catalysis Science & Technology Accepted Manuscript

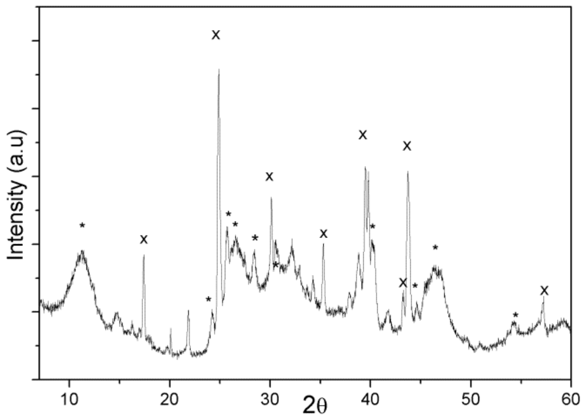

Fig.1 XRD pattern for NiMo-as bulk sulfide catalyst. Symbol ∗: peaks corresponding to MoS_2 and symbol ×: peaks corresponding to Ni_3S_2

molybdenum occupies tetrahedral sites, was strongly predominant in NiMo-b-ca and a mixture of the α and β-phases are present in NiMo-a-ca. Peaks corresponding to the Ni or Mo simple oxides were not identified in either pattern, suggesting that the calcined materials are non-stoichiometric mixed-oxides with excess nickel. Yin at al.[40] have shown that pure nickel molybdates with the β-phase structure may be obtained with Ni:Mo ratios up to 1.5. Due to the fact that our Ni:Mo ratios were slightly higher than 1.5, the presence of a small amount of an X-ray invisible nickel-containing phase, such as nickel oxide, may not be completely excluded.

It is known that calcined, NiMo-containing precursor salts where molybdenum has tetrahedral coordination result in the β-nickel molybdate phase formation, after calcination at temperatures between 623 and 723 K [41, 42]. This is also the case of mixed oxides obtained from the ϕ_y[40] crystal structure, but the β → α transformation takes place at about 473 K on cooling [43]. It has been proposed[43] that the β phase is stabilized when excess nickel is present. This may partly explain the presence of the β phase in both materials, but does not explain the difference between them, since Ni:Mo ratios were very similar in both cases. An alternative explanation for β-nickel molybdate phase stabilization could be the formation of very small crystals after calcination which, due to a surface free energy effect, could favour the thermodynamically less stable bulk phase, similarly to what was previously reported for zirconia [36], provided the surface free-energy of the α phase is larger than that of the β phase. In the presence case, this could be attributed to the use of nickel sulphate, rather than nitrate, in the preparation of NH_4-NiMo-b.

The DRX pattern of the NiMo-as sulphide is shown in Fig 1. Peaks corresponding to MoS_2 (ICSD-601647) and Ni_3S_2 (ICSD-654935) compounds were identified in the sulphides.

The Scherrer equation was employed to estimate the MoS_2 particle size, D, in the c-axis direction:

$$D = \frac{k\lambda}{\beta\cos\theta} \qquad (2)$$

where k is the shape factor equal to 0.76 [44], λ is the wavelength used, β is the FWHM of the (0 0 2) peak appearing at 11.3°. A D value of 22.8 Å was obtained, correspoding to a 3.7 average degree of stacking of the MoS_2 layers, considering the (0 0 2) interplanar distance as 6.15 Å. The peaks attributed to Ni_3S_2 are very thin, implying the presence of relatively large crystals of this substance in the catalyst. Possibly, these large nickel sulphide crystals arise from sulphidation of the X-ray invisible nickel oxide species discussed above.

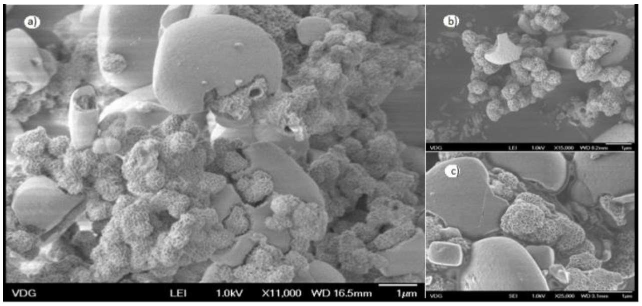

Fig. 2 SEM Images of a) NH_4-NiMo-a; b) NiMo-a-ca; c) NiMo-as

3.1.2. Textural properties. The calcined solids NiMo-a-ca and NiMo-b-ca presented BET surface areas of 30 and 95 m2/g, respectively. The predominance of β-nickel molybdate has been reported to favour the surface area for this material [45]. So these areas are consistent with the DRX patterns reported here and also with the idea expressed in section 3.1.1, that a smaller crystallite size may stabilize the thermodynamically less stable β phase. The N_2 adsorption isotherms and pore size distributions for both mixed-oxides are presented in figure S3 of the supplementary material.

The corresponding sulphide catalysts, analysed after the catalytic test, as explained under section *2.5*, have surface areas of 35 and 44 m^2/g, for NiMo-as and NiMo-bs, respectively. Fig. S4 shows the nitrogen adsorption isotherms for NiMo-as and NiMo-bs catalysts and their corresponding pore size distribution obtained from the isotherm adsorption branch. The steep rise in the isotherm at values of relative pressure close to 1.0, indicates the occurrence of capillary condensation in macropores or in interparticle voids, but the existence of a pronounced hysteresis loop denotes the existence of mesopores as well. From the pore sizes distributions, these mesopores have their maximum concentration near the mesopore-micropore limit (20 Å) and the porosity seems to extend into the micropore region. So the sulphidation process, followed by use in the catalytic reaction, caused a very pronounced change in the textural properties of the solids.

3.1.3. SEM and HR-TEM. The SEM image of the NH4-NiMo-a layered precursor is shown in Figure 2a. This material presents a unique morphology, defined predominantly by agglomerated coral-like particles, having similar shapes and sizes. Many of them seem to grow out of fragments of larger eggshell-like particles with rough surfaces. Figs.2b and 2c show that essentially the same morphology is maintained after calcination and sulphidation followed by the catalytic test.

Figs. 3a and 3b show representative high-resolution TEM images of NiMo-as and the alumina-supported NiMo catalyst, respectively, taken in high resolution mode. The presence of randomly distributed lamellar particles, typical of MoS_2, is clearly distinguished. The slabs are typically curved and individual particles are present with varying stacking degrees. The interlayer distance is ca. 6 Å, which is approximately the distance (6.15 Å) between (0 0 2) planes in the MoS_2 crystal structure.

Catalysis Science & Technology Accepted Manuscript

This journal is © The Royal Society of Chemistry [year]

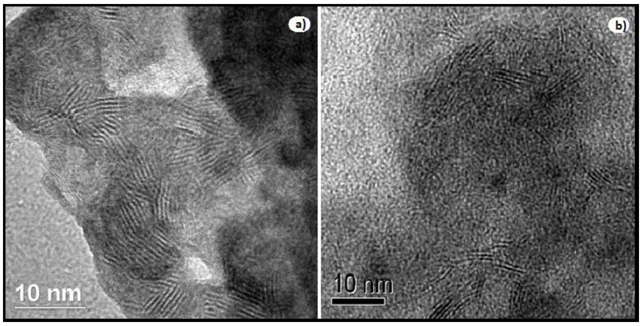

Fig. 3 HR-TEM images for a) NiMo-as and b) NiMo/Al$_2$O$_3$.

In the supported catalyst a higher dispersion of MoS$_2$ particles is appreciated. The distribution for sulphide slabs stacking degrees and average length (see figure S5a and S5b) were obtained from measurements for about 120 particles (498 layers) in different images. The values are summarised in Table 1. Notice that the average stacking number (ASN) determined from the TEM measurements is in quite good agreement with the one determined from Scherrer's equation for NiMo-as.

Table 1 Distribution of slabs stacking degrees and average length from measurements in the HR-TEM images of NiMo-as and NiMo/Al$_2$O$_3$ catalysts.

Catalyst	L (Å)[(a)]	ASN[(b)]	A_s (m^2 g^{-1})[(c)]
NiMo-as	29	3.9	404
NiMo/Al$_2$O$_3$	36	3.1	-

[(a)]Average length; [(b)]average stacking number; [(c)] surface area estimated from slab geometry.

The apparent surface area of the MoS$_2$ slabs could be estimated considering the particles as hexagonal prisms with base diameter equal to the average slab length. The prism height is taken to be equal to the distance between slabs, d$_{(002)}$, multiplied by the average stacking number. The result is shown in Table 1 and it is much larger than the surface area measured by nitrogen physisorption, indicating that a large portion of the slabs is inaccessible to the gas phase. This is due to the fact that the sulphide particles in the unsupported catalyst seem to be comprised of aggregates of intertwined MoS$_2$ slabs.

A similar analysis was not made in the case of the supported NiMo catalyst, since in supported systems it is difficult to quantify the amount of single-slab crystallites without the use of special techniques [46]. However, it is interesting to point-out that the differences in slab length and degree of stacking between the supported and the unsupported catalyst is not as large as might have been expected. The main effect of the support in the present case seems to have been the breakdown of the large MoS$_2$ slab aggregates observed in the unsupported catalyst.

An atomic structural study has been done on HR-TEM images taken for the NiMo-as catalyst using Digitalmicrograph and SADP Tools [47], as shown in Fig. 4. A zoom from a randomly chosen square region in Fig. 4a is presented in Fig. 4b. The FT of the latter is shown in Fig 4c. Finally, Fig. 4d shows the intensity distribution in the image of Fig. 4c as an inverse function of reciprocal space. This image was obtained doing a circular integration in the image of Fig. 4c and thereafter, the background was removed.

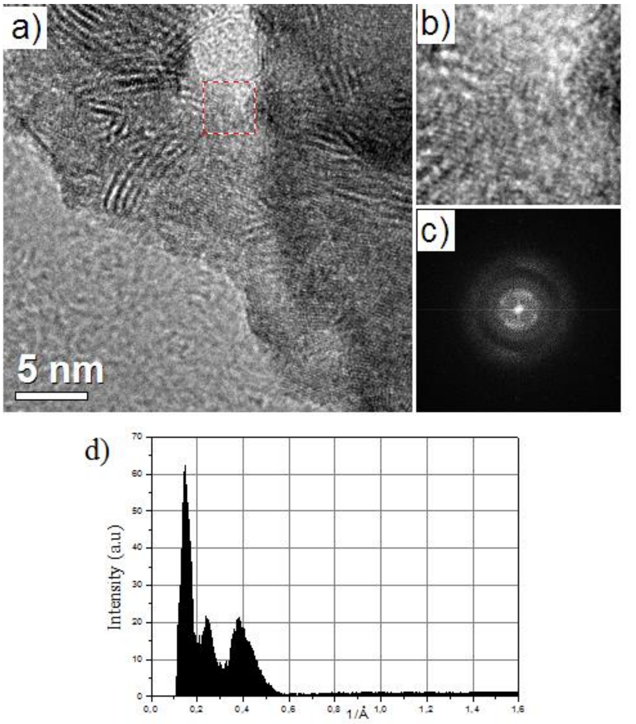

Fig.4 a) HR-TEM image for NiMo-as catalyst; **b)** Zoom of square selected region in a); **c)** TF of region b); **d)** Intensity distribution of c) in the reciprocal space

The first peak (centred near 0.16 Å $^{-1}$ or 6.13 Å in the real space) corresponds to the contribution of real-space of a 6.15 Å interlayer distance, assigned to the (0 0 2) planes in the MoS$_2$ crystal structure.

The second peak (ca. 0.24 Å $^{-1}$ or 4.08 Å), about three times less intense than the first one, was attributed to the diffraction scattering originated from (1 0 1) planes of Ni$_3$S$_2$ clusters, which have 4.08 Å interplanar distance in the real space. Interplanar distances in this region are completely absent in the MoS$_2$ crystal structure. The wider last peak (extending from about 0.37 to 0.43 Å $^{-1}$ or from 2.70 to 2.33 Å), could be due to the contribution of the (1 0 0), (1 0 1), (1 0 2) and (1 0 3) family of planes of the MoS$_2$ crystal structure, besides other planes from Ni$_3$S$_2$ structure. In summary, the MoS$_2$ crystal structure does not have any interplanar distances that match the second peak in Fig. 4d, only the (1 0 1) plane of Ni$_3$S$_2$ matches this peak.

It should be noticed that, differently from other work [48, 49], well ordered Ni sulphide structures were not identified in our HR-TEM images. So, the second peak contribution, Fig. 4d, could be due to a poorly ordered Ni$_3$S$_2$ phase interspersed in-between the MoS$_2$ crystallites. This seems to contradict the XRD results, which revealed the existence of sharp nickel sulphide reflections indicative of the presence of relatively large nickel sulphide particles in this catalyst. This could be due to the fact that, although the XRD nickel sulphide peaks are sharp, their area contribution is small, so that the particles responsible for these peaks represent a small portion of the nickel present in the sample.

3.1.4 X-Ray Absorption. The XANES region of the X-ray absorption spectrum of the NiMo-as and NiMo-bs catalysts at the nickel edge shows features similar to those of a commercial Ni3S2 sample used as a standard, as presented in Fig. S6. In

Catalysis Science & Technology Accepted Manuscript

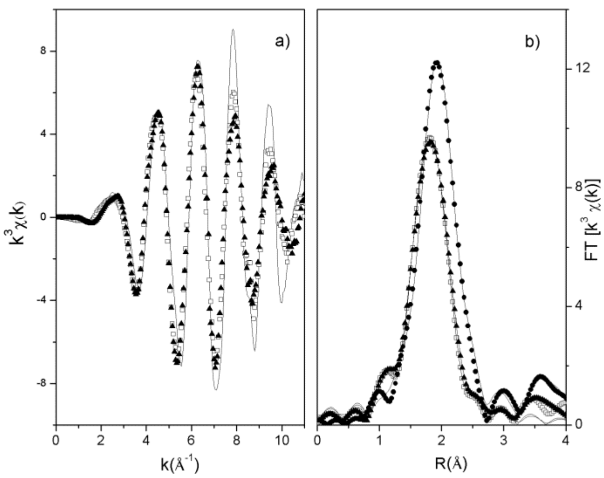

Fig.5 a) EXAFS oscillation at the Ni edge for □ NiMo-as, ▲NiMo-bs and commercial Ni_3S_2 (solid line). **b)** k^3-weighted TF from EXAFS oscillation □ NiMo-as, ▲NiMo-bs, ● commercial Ni_3S_2 and their corresponding fittings in R-space (solid lines)

particular, the position of the absorption edge is not shifted in the spectra of the catalysts with respect to Ni_3S_2 , showing that the catalysts were not oxidized during manipulation. It should be said that the conventional NiMo/Al_2O_3 was partially oxidized (XANES not shown), probably due to the manipulation procedure after the catalytic test or sample preparation for XAS analysis.

Figures 5a and 5b show, respectively, the k^3-weighted EXAFS oscillations and the corresponding FT spectra, extracted from the Ni-edge absorption spectra, for NiMo-as, NiMo-bs and the Ni_3S_2 standard. The first FT peak is clearly narrower for the catalysts than for the standard. This is attributed to the fact that both the first coordination shell Ni-S path and the second coordination shell Ni-Ni path contribute to the first peak of the FT spectrum of Ni_3S_2 and that nickel sulphide is present in the catalysts, at least partly, as small clusters with an incomplete second coordination shell.

The EXAFS spectra were fitted in R-space, with paths generated from the Ni_3S_2 structure (ICSD 23114) using the Artemis software. Table 2 shows the parameters obtained from the simulation for both the Ni_3S_2 bulk material for both the Ni_3S_2 bulk material and used catalysts NiMo-as and NiMo-bs. The small values for the fitting parameter R_{factor} demonstrate the good quality of the simulations.

Table 2 EXAFS parameters from Ni K-edge simulation for sulphides

Catalyst	Coordination Shell	*C.N*	*R*(Å)	σ^2(Å^2).10^3	R-*factor*(%)
NiMo-as	Ni-S	4.2±0.3	2.24±0.01	6.2±0.8	0.04
	Ni-Ni	1.5±0.4	2.51±0.02	9[a]	
NiMo-bs	Ni-S	4.4±0.3	2.25±0.01	6.8±0.8	0.07
	Ni-Ni	1.1±0.4	2.54±0.01	9[a]	
Ni_3S_2	Ni-S	4	2.26±0.01	8.0±1.0	0.5
	Ni-Ni	4	2.49±0.01	9.0±1.0	

[a] The Debye-Waller for the second shell was fixed in the simulation of the unsupported catalysts to the value obtained for the Ni_3S_2 reference.

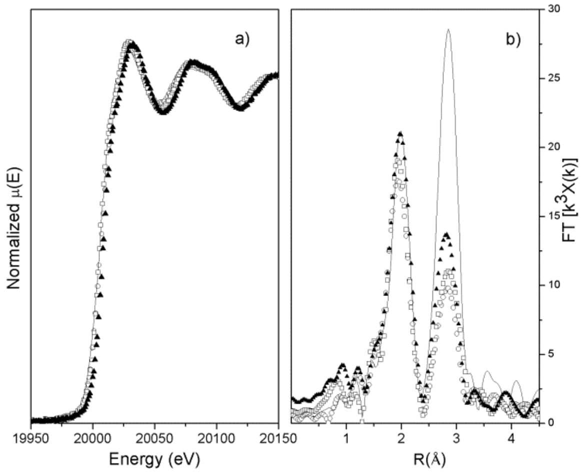

Fig. 6. a) Mo K-edge XANES region and **b)** Mo K-edge k^3-weighted TF from EXAFS oscillation □ NiMo-as, ▲NiMo-bs, ○ NiMo/Al_2O_3 and commercial MoS_2 (solid line)

The Ni second sphere coordination number shown in Table 2 equals approximately 1 for the unsupported catalysts, implying that nickel would be present in small sulphide clusters. This is in agreement with all analysed TEM images which do not indicate the presence of large nickel sulphide crystallites, but seems to be in conflict with the XRD results that display thin Ni_3S_2 diffraction peaks. As mentioned before, the explanation could be that, although these thin diffraction peaks are intense, their area contribution is small, so that only a small fraction of the nickel sulphide is visible in the DRX patterns. An alternative hypothesis is that nickel is present as an atomically dispersed species, such as in the so-called NiMoS phase [50], coexisting with large nickel sulphide crystallites as reported recently for Co-promoted unsupported systems [21]. Again, it has to be noticed that large Ni_3S_2 crystals were not observed in our TEM images and, furthermore, if a large portion of the nickel was atomically dispersed, a peak due to the NiMoS species would be expected at 2.85 Å in the Fourier-transformed Ni K-edge EXAFS spectra of the catalysts. This does not necessarily imply that the NiMoS phase is absent from our catalysts, since it may have remained undetected because the corresponding nickel signal was overwhelmed by the more abundant, nearly amorphous Ni_3S_2-like phase.

In Figs. 6a and 6b are shown the Mo-K edge XANES region and the k^3-weighted FT spectrum of NiMo-as, NiMo-bs, NiMo/Al_2O_3 and of a MoS_2 standard. It can be seen from Fig. 6a that the Mo-K white line feature typical of the oxide phase (MoO_3) in the XANES region is completely absent and the XANES region is very similar to that of the MoS_2 pattern, which is a strong indication of Mo complete sulphidation using the activation method described here. In Table 3 the parameters for the EXAFS. simulation of the k^3 weighted EXAFS spectra are shown. The average sizes of the molybdenum sulphide crystallites were determined from the second shell Mo-Mo coordination numbers using the Shido and Prins correction [51] and are shown in the "particle diameter" column in Table 3.

Catalysis Science & Technology Accepted Manuscript

Table 3 EXAFS parameters from Mo K-edge simulation for sulphides

Catalyst	Coord. Shell	*C.N*	*R*(Å)	σ^2(Å^2).10^3	Particle Diameter (Å)^a	R-*factor* (%)
NiMo-as	Mo-S	6.7±0.5	2.41±0.01	3.6±0.5		0.7
	Mo-Mo	4.5±0.9	3.17±0.01	4.1±0.1	56	
NiMo-bs	Mo-S	6.4±0.7	2.40±0.05	3.1±0.7		0.7
	Mo-Mo	3.8±0.9	3.16±0.01	3.2±1.1	33	
NiMo/Al$_2$O$_3$	Mo-S	6.1±1.0	2.40±0.01	3.5±1.0		1.5
	Mo-Mo	3.5±1.7	3.15±0.01	3.9±2.2	26	
MoS$_2$	Mo-S	6	2.40±0.04	3.2±0.3		1.2
	Mo-Mo	6	3.16±0.04	2.4±0.2		

^{a} Calculated from ref.51

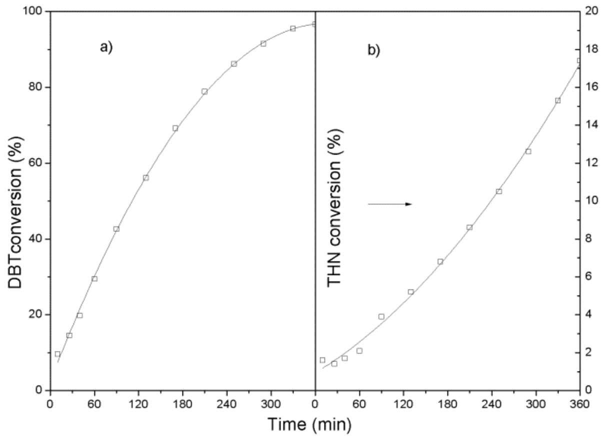

Fig.7 Conversion *vs* time for a) DBT and b) THN in the catalytic test for NiMo-as bulk catalyst

The particle diameter, which actually corresponds to MoS$_2$ slab length, are in qualitative agreement with the ones obtained from TEM, bearing in mind the uncertainty in the value of the second shell Mo-Mo distances. This confirms that there is not a very large difference in size between the MoS$_2$ crystallites in the unsupported and the alumina-supported catalyst. In terms of particle morphology, the main effect of the support here seems to have been the breakdown of the large sulphide slab aggregates present in the unsupported catalyst into smaller ones.

3.2 Catalytic tests

The curves for DBT and THN (tetralin) conversion *vs.* time for NiMo-as are shown in Fig. 7. The initial rate of DBT conversion is higher than that of THN hydrogenation. A clear upward curvature of THN conversion vs. time is observed, indicating an acceleration of the reaction.

Figs. 8a and 8b show product yield vs. conversion curves, respectively in the HDS of DBT and in THN hydrogenation. The points corresponding to THN hydrogenation follow quite accurately straight lines, whereas the curve for biphenyl (BPH) formation has a slight downward curvature, while that for cyclohexylbenzene CHB formation has an upward curvature, indicating the occurrence of BPH hydrogenation to CHB.

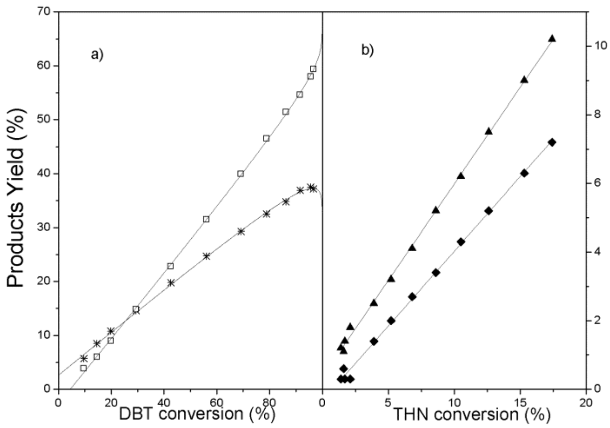

Fig.8 Products yield *vs* reactant conversion for NiMo-as bulk sulfide catalyst. **a)** □ CHB and * BPH and first order fit (solid lines). **b)** ♦ cis-decalin and ▲trans-decalin and zero order fit (solid lines).

For the purpose of studying catalyst selectivity, a network of irreversible pseudo-first order reactions was assumed for the HDS of DBT, as shown in scheme 1, noticing that the reaction was carried-out under constant hydrogen pressure

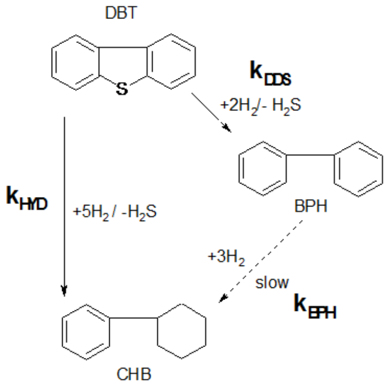

Scheme 1 Kinetic network proposed for HDS of DBT

In this scheme CHB represent cyclohexylbenzene and BPH represents biphenyl. Within this scheme, the rates of conversion of each substance are given by:

$$\frac{dY_{DBT}}{dt} = -(k_{DDS} + k_{HYD})Y_{DBT} \quad (3)$$

$$\frac{dY_{CHB}}{dt} = k_{HYD}Y_{DBT} + k_{BPH}Y_{BPH} \quad (4)$$

$$\frac{dY_{BPH}}{dt} = k_{DDS}Y_{DBT} - k_{BPH}Y_{BPH} \quad (5)$$

where Y_i is the amount in moles of substance *i* in the reaction mixture per mole of DBT initially present in the system, i.e. it represents the yield for substance *i* at any given time.

It is not difficult to demonstrate that the yields are expressed, as a function of DBT conversion, *x*, respectively by equations (6) and (7) below:

Catalysis Science & Technology Accepted Manuscript

$$Y_{BPH} = \frac{k_{DDS} / k_0}{k_{BPH} / k_0 - 1} [1 - x - (1 - x)^{k_{BPH} / k_0}] \tag{6}$$

$$Y_{CHB} = x - Y_{BPH} \tag{7}$$

where the acronyms DDS, HYD and BPH represent, respectively, the *direct desulphurisation route*, that leads directly from DBT to BPH, the *prehydrogenation route*, that leads from DBT to CHB, and BPH *hydrogenation*, that leads from BPH to CHB and $k_o = k_{DDS} + k_{HYD}$. A non-linear least-squares procedure implemented in Mathematica [52] was used to extract k_{DDS}, k_{HYD} and k_{HBP} values from product yield vs. DBT conversion data. The curves in Fig. 8a (solid lines) represent the best fit with this simple model. Curves for the other catalysts studied, equivalent to Figs. 7 and 8, are shown in Figs. S7 to S9 in the supplementary material.

In the case of tetralin conversion, no evidence was found for interconversion between the isomeric products cis- and trans-decalin, as straight lines were obtained when the yield of each product was plotted against tetralin conversion. In this case, selectivity was analyzed simply in terms of the ratio of initial rates of formation of both products.

The activity and selectivity results of catalytic tests for simultaneous HDS of DBT and HDA of THN are shown in Table 4. The values for the overall selectivity to HDA relative to HDS (r_{HDA}/r_{HDS}) are shown in the last column.

Table 4 Results of catalytic tests

Catalyst	[a] $r_{HDS}.10^7$ (mol/g.s)	[a] $r_{HDA}.10^7$ (mol/g.s)	[b] *cis-/trans* -	[c] k_{BPH}/k_{DDS}	[c] k_{HYD}/k_{DDS}	r_{HDA}/r_{HDS}
NiMo-as	31.8	10.4	0.9	0.1	1.5	0.3
NiMo-bs	26.3	5.3	0.8	0.1	1.4	0.2
NiMo /Al_2O_3	17.3	6.3	0.3	-	0.4	0.4
NiMoP /Al_2O_3	29.5	16	0.4	0.2	0.7	0.5
NiMo-bs[d] (Toluene)	27.1			0.1	1.6	
NiMo-bs[e] (Thiophene)		25.3	0.5			

[a] r_{HDS} and r_{HDA} initial reaction rates for DBT HDS and THN HDA, respectively. [b] Selectivity ratio for THN HDA isomeric products from initial rates. [c] Selectivity for DBT HDS products determined from pseudo-first order kinetic model (see text). [d] Catalytic test where THN was replaced by the same volume of Toluene. [e] Catalytic test where DBT was replaced by thiophene (200 wppm sulphur). See Section 2.7

Besides the results for NiMo-as and NiMo-bs, the table also reports results obtained with a NiMo/Al_2O_3 catalyst prepared in our lab, as described in [32], with a 1:1 Ni/Mo ratio and for a commercial NiMoP/Al_2O_3 hydrotreating catalyst.

From the r_{HDS} and r_{HDA} results shown in Table 4, the NiMo-as catalyst is seen to be more active than NiMo/Al_2O_3 and to have the same activity as the commercial NiMoP catalyst in the HDS reaction and to be more active than NiMo/Al_2O_3 and less active than NiMoP in the HDA reaction, when activities are reported per gram of catalyst, but it will certainly have a smaller activity on an active metal basis. However, since the bulk sulphide materials are much denser than the supported ones, if the activity is reported per catalyst volume, as is commonly done by catalyst manufacturers, their activity will certainly be higher than those of the supported catalysts.

The NiMo-as catalyst showed a slightly higher activity for HDS than, and about twice the activity for HDA as, the NiMo-bs catalyst, which was prepared using nickel sulphate instead of the nitrate, however, their selectivities for the products of both reactions are very similar.

As shown in Table 4, when the NiMo-bs catalyst was evaluated with toluene replacing THN, the values of activity and selectivity were very close for DBT HDS. On the other hand, when thiophene replaced DBT in the standard test, the NiMo-bs catalyst presented a higher HDA activity by a factor of five. In this last case, the selectivity for *trans*-decalin formation increased markedly. These tests indicate that, in simultaneous reactions, the HDA of THN is much more inhibited by DBT than by thiophene, implying that DBT competes strongly with THN for the hydrogenation sites. Additionally this fact is evidenced by the absence of an upward curvature in THN HDA when DBT was replaced by thiophene. This also shows that the upward curvature in THN HDA in the presence of DBT is not caused by promotion of the HDA by hydrogen sulphide, but rather by replacement of a strong competitor, DBT, by the weaker one, hydrogen sulphide. Furthermore, DBT inhibits more strongly the sites responsible for trans-decalin formation.

In contrast, the HDS of DBT was insensitive to the nature of the aromatic hydrocarbon, suggesting that these cannot favourably compete with DBT for the HDS sites, given the fact that the gas phase basicity of THN (782.1 kJ mol^{-1}) is larger than that of toluene (756.3 kJ mol^{-1}) [53], so THN is expected to adsorb more strongly than toluene on sulfur vacancies.

The selectivity for the HYD route in HDS (direct CHB formation) was much higher with the bulk catalysts than with the supported ones, which were selective for the DDS route (BPH formation). This is in agreement with what is known in the literature [22]. Between the supported catalysts, NiMoP/Al_2O_3 was more selective for the DDS route. It should be said that the DBT conversion achieved was smaller in the case of the NiMo/Al_2O_3 catalyst prepared in our lab, so the k_{BPH}/k_{DDS} ratio was not reported in Table 4 since the reliability of this value in not guaranteed with the kinetic model employed.

Both unsupported catalysts were significantly more selective for cis-decalin than the supported ones in the HDA of THN.

It is very interesting to observe, from the r_{HDA}/r_{HDS} ratios that, although being more selective for the HYD route in HDS, the HDA/HDS selectivity was actually somewhat smaller for the unsupported catalysts than for the supported ones. The similarity in selectivity to HDA as compared to HDS is also apparent from the k_{BPH}/k_{HDS} values, which were similar for both supported and unsupported catalysts.

4 Discussion

The results obtained confirm the high selectivity of bulk NiMo sulphide catalysts for the HYD pathway of dibenzothiophene HDS relative to supported ones. One obvious explanation for this would be that, in unsupported catalysts, separate molybdenum

Catalysis Science & Technology Accepted Manuscript

This journal is © The Royal Society of Chemistry [year]

and nickel phases exist, while in supported systems the nickel is largely associated with the so-called NiMoS phase [3], thus the mechanism of nickel promotion would be different in each case. Most of the support for the NiMoS model has come from studies with supported catalysts, but several authors have questioned its application to unsupported systems [3, 4, 21, 54]. For separate molybdenum and nickel sulphide particles, the so-called contact synergy mechanism has been proposed [3, 54] and references there in. This model supposes that hydrogen is dissociated on the divalent metal sulphides and spills over to the MoS_2 crystallites, where the organic reactant is adsorbed [48, 54]. Recent work by Ramos et al. [21] proposes that in unsupported Co_9S_8/MoS_2 systems, the synergy effect is due to the interface formed by interaction between the edge plane of the MoS_2 crystallites and the (111) plane of Co_9S_8.

Our TEM results clearly show the presence of nickel sulphide clusters in close contact with the MoS_2 particles, so this mechanism could contribute to enhance hydrogen flow to the active sites and thus explain the higher selectivity of the unsupported catalysts for the HYD route in HDS. This does not explain, however, why the HDA/HDS activity ratio, as measured using DBT and THN as model compounds and also the k_{BPH}/k_{DDS} ratio, appear to be nearly insensitive to the support effect.

One way in which selectivity effects in HDS are discussed in the literature has to do with the morphology of the sulfide crystallites [48, 55, 56]. One of the first models was proposed by Chianelli [57].

In the rim-edge model [57], developed for unsupported, unpromoted MoS_2, it was proposed that the HYD pathway would be favoured on sites present at the basal edges of the hexagonal prisms assumed to constitute the sulphide particles (rim sites). On the other hand, the DDS route would occur on sulphur vacancies both at the rim sites and on sites present at the edges of the sulphide slabs located at the lateral faces of the prisms (edge sites). Consequently, a higher average slab stacking number would be expected to favour the DDS route. More recently, their results with supported unpromoted and Co-promoted MoS_2 led them to conclude that interactions with the support are as important as the stacking degree of the MoS_2 slabs as the determining factor in these catalysts [46]. In their new model, single slabs in direct contact with the alumina may be classified as type I rim sites, with low selectivity for the HYD route in HDS; in stacked slabs, type II rim and edge sites would exist with respectively high and low selectivity for the HYD route. In order to apply this model to our results we would have to assume that single slabs constitute a large fraction of the molybdenum sulphide in the alumina-supported catalyst but remained undetected by TEM, as the observed stacking degrees were not very different in the supported and in the unsupported catalysts (cf. Table 1). Furthermore, this model offers no explanation to our selectivity results, as far as the difference in support effects on the HYD route in dibenzothiophene HDS and the HDA of tetralin is concerned.

We believe the simplest explanation for our selectivity results is that the HDA reaction does not occur only on the same sites responsible for the HYD route in DBT HDS, but also on the sites responsible for the DDS route. Adsorption of DBT for the DDS route is thought to occur in η^1 mode by the sulphur atom on sulphur vacancies located at the edge of the promoted sulphide crystallites [38], especially at corner sites [58], while the HYD route would involve a flat η^6 adsorption, not necessarily on sulphur vacancies, but possibly on the so-called “brim sites” proposed by Tøpsoe et al. [58], located near the edge of terminal basal planes of the sulphide stacks, which have metallic character. It is commonly assumed that hydrogenation of aromatic hydrocarbons occurs by essentially the same mechanism as in the hydrogenation of DBT, but recently, in a DFT study of benzene adsorption on nickel-promoted tungsten sulphide, Koide et al. [59] have shown that this compound may adsorb in η^2 mode on coordinatively unsaturated tungsten corner sites located next to a nickel atom. It is relevant that corner sites have been found by Lauritsen et al.[58] to be the preferential ones for DBT chemisorption on model CoMoS clusters. Therefore, the idea that the same type of sites may be involved in the DDS route for DBT HDS and partially in the hydrogenation of aromatic hydrocarbons finds some support in the literature.

Even though the HYD/DDS selectivity is significantly different for unsupported and supported catalyst and the HDA/HDS ratio is practically the same, cis- and trans-decalin formation were affected to different extents by the support effect. Table 5 shows the initial rates of formation of the different HDS and HDA products, calculated from the data in Table 4.

Table 5 Initial rates of formation for HDS and HDA products.

Catalyst	r_{HDS}		r_{HDA}	
	r_{HYD}	r_{DDS}	r_{cis-}	r_{trans-}
NiMo-as	18.9	12.6	4.9	5.5
$NiMo/Al_2O_3$	4.9	12.4	1.4	4.8
ratio[a]	3.8	1.02	3.5	1.14

[a] ratio between r_X values for both catalysts.

It is clear that cis-decalin formation is influenced by the support effect essentially to the same extent as CHB formation, and trans-decalin formation is influenced to essentially the same extent as BPH formation. It is tempting to suggest that CHB and cis-decalin formation on one hand, and BPH and trans-decalin formation on the other, occur on the same types of site and involve related intermediates.

Shabtai et al [60] have proposed that the high selectivity for trans-decalin formation during naphthalene hydrogenation on sulphide catalysts, as opposed to metals, is due to the possibility of edge-wise adsorption of the ring system on double or multiple sulphur vacancies, allowing the addition of hydrogen from opposite sides of the C9-C10 ring position. On the other hand, the DDS route for HDS is supposed to involve σ-adsorption (η^1 adsorption) of the sulphur compound on single vacancies. If trans-decalin formation and the DDS route in HDS are related, one could imagine that a vertically adsorbed σ-bonded intermediate would be involved in the addition of hydrogen from either side of the partially hydrogenated tetralin ring.

Similarly, the HYD route in DBT HDS has been proposed to occur in η^6 adsorption mode [38]. It may be speculated that cis-decalin-selective THN HDA involves a similarly flatly adsorbed species that would favour addition of hydrogen from a single side of the aromatic ring. The preferential suppression of both the HYD route in DBT HDS and cis-decalin formation in THN HDA

Catalysis Science & Technology Accepted Manuscript

when moving from the unsupported to the supported catalyst may be attributed to the support interaction effect present in the latter, as proposed by Berhault et al.[46], since the opposite effect would be expected only on the basis of stacking degree. It is also conceivable that a difference between the kinds of synergetic effect in supported and unsupported catalysts (e.g. NiMoS phase vs. contact synergy) may influence the preferred adsorption mode of the reactants.

It is interesting that there is an increase in cis/trans decalin ratio when thiophene is replaced by DBT as a competitor for THN HDA, implying that, following the proposed model, DBT competes more effectively with THN for sulphur vacancies on edge or rim sites, than for planar adsorption on metal-like sites.

5 Conclusions

Nickel-ammonium layered molybdates have been synthesised using a co-precipitation method, and the so-called ϕ_y phase was obtained, with Ni/Mo atomic ratios in the order of 1.5. After calcination, nickel molybdates with excess nickel were obtained with different surface areas and proportions of the α and β phases, depending on the nickel precursor salt used (nitrate or sulphate).

The catalysts obtained by sulphidation of these mixed-oxides in liquid phase were comprised of intertwined molybdenum sulphide crystallites with average stacking degree of about 4 interspersed with a disordered nickel sulphide phase.

Evaluation of the catalysts in the simultaneous HDS of DBT and tetralin HDA, revealed that they were much more selective than supported NiMo catalysts, both for the HYD route in DBT HDS and for cis-decalin formation in the HDA of tetralin.

With basis on the current models for hydrotreating catalysts it is proposed that the HYD route in DBT HDS and cis-decalin formation in tetralin HDA on one hand, and the DDS route in DBT HDS and trans-decalin formation in tetralin HDA on the other, involve related active sites and adsorbed intermediates.

Acknowledgments

The authors would like to thanks PETROBRAS for the financial support**.** To Laboratório Nacional de Luz Síncrotron (LNLS) for project XAS XAFS1- 9136, XAFS2 10161, D10B-XPD 9914 and Laboratório Nacional de Nanotecnología LNANO for HR-TEM 10300 and 11528 approvals. NUCAT (COPPE/UFRJ - Brazil) for XRF, Laboratório Multiusuário (IQ/UFRJ - Brazil) for XRD. J.-G. Eon thanks CNPq for support in this work.

Notes and references

[a] *Instituto de Química, Universidade Federal de Rio de Janeiro, Av. Athos da Silveira Ramos, 149 Bloco A, CEP, 21941-909, Rio de janiero, RJ, Brasil. E-mail: farojr@iq.ufrj.br*

[b] *Grupo Catalizadores y Adsorbentes, Universidad de Antioquia, A. A. 1226 , Medellín, Colombia.*

[c] *Laboratório Nacional de Nanotecnologia, Centro Nacional de Pesquisa em Energia e Materiais, 13083-970, Campinas, Brasil.*

[d] *Instituto de Química, Universidade do Estado de Rio de Janeiro, Rua São Francisco Xavier, 524, CEP, 20550-900, Rio de janiero, RJ, Brasil.*

† Electronic Supplementary Information (ESI) available: XRD patterns of layered precursor and mixed-oxides; N_2 adsorption isotherms and pore distribution of mixed-oxides and sulphides; distribution for slab stacking and lenghts of an unsupported and a supported catalyst; XANES spectra in the Ni K-edge for unsupported catalysts and a standard reference; Products yield *vs* reactant conversion for an unsupported and two supported catalysts. See DOI: 10.1039/b000000x/

‡ Footnotes should appear here. These might include comments relevant to but not central to the matter under discussion, limited experimental and spectral data, and crystallographic data.

1. T. C. Ho, *Catal. Today*, 2004, **98**, 3.
2. I. V. Babich and J. A. Moulijn, *Fuel*, 2003, **82**, 607.
3. H. Topsøe, Clausen, B.S., and Massoth, F. E., *Hydrotreating Catalysis Science and Technology*, 1 edn., Springer-Verlag New York 1996.
4. S. Eijsbouts, S. W. Mayo and K. Fujita, *Appl. Catal. A*, 2007, **322**, 58.
5. B. C. Gates and H. Topsøe, *Polyhedron*, 1997, **16**, 3213.
6. FuelRegulations, Ecopoint Inc., http://www.dieselnet.com/standards/fuels.php.
7. K. B. Sidhpuria and P. A. Parikh, *Bull. Catal. Soc. Ind.*, 2004, **3**, 67.
8. A. Stanislaus, A. Marafi and M. S. Rana, *Catal. Today*, 2010, **153**, 1.
9. Z. Le, P. Afanasiev, D. Li, X. Long and M. Vrinat, *Catal. Today*, 2008, **130**, 24.
10. G. Alonso, G. Berhault, A. Aguilar, V. Collins, C. Ornelas, S. Fuentes and R. R. Chianelli, *J. Catal.*, 2002, **208**, 359.
11. T. C. Ho, *Catal. Today*, 2008, **130**, 206.
12. J. Bocarando, R. Huirache-Acuña, W. Bensch, Z. D. Huang, V. Petranovskii, S. Fuentes and G. Alonso-Núñez, *Appl. Catal. A*, 2009, **363**, 45.
13. P. Afanasiev, *C. R. Chim.*, 2008, **11**, 159.
14. D. Genuit, P. Afanasiev and M. Vrinat, *J. Catal.*, 2005, **235**, 302.
15. S. L. Soled, Sabato, M.,Krycak, R., Vroman, H., Ho, T. E Riley, K., *United State Patent*, 2000, **6156695**.
16. Y. Gochi, C. Ornelas, F. Paraguay, S. Fuentes, L. Alvarez, J. L. Rico and G. Alonso-Núñez, *Catal. Today*, 2005, **107-108**, 531.
17. L. Wang, Y. Zhang, Y. Zhang, Z. Jiang and C. Li, *Chem. Eur. J.*, 2009, **15**, 12571.
18. D. Levin, S. L. Soled and J. Y. Ying, *Inorg. Chem.*, 1996, **35**, 4191.
19. M. J. Peltre and H. Pezerat, *J. Less Common Met.*, 1974, **36**, 61.
20. D. Levin and J. Y. Ying, in *3rd World Congress on Oxidation Catalysis*, 1997, vol. 110, pp. 367.
21. M. Ramos, G. Berhault, D. A. Ferrer, B. Torres and R. R. Chianelli, *Catal. Sci. Technol.*, 2012, **2**, 164.
22. N. Hermann, M. Brorson and H. Topsøe, *Catal. Lett.*, 2000, **65**, 169.
23. B. Yoosuk, J. H. Kim, C. Song, C. Ngamcharussrivichai and P. Prasassarakich, *Catal. Today*, 2008, **130**, 14.
24. J. Ren, A. Wang, J. Tan, G. Cao, C. Liu, Y. Li, M. Lu, Y. Hu and S. Q. Y. T. a. C. Y. Dongyuan Zhao, in *Stud. Surf. Sci. Catal.*, Elsevier, 2007, vol. Volume 165, pp. 721.
25. H. Farag, *J. Colloid Interface Sci.*, 2010, **348**, 219.
26. V. Rabarihoela-Rakotovao, S. Brunet, G. Perot and F. Diehl, *Appl. Catal. A*, 2006, **306**, 34.
27. D. D. Whitehurst, T. Isoda and I. Mochida, in *Adv. Catal.*, Academic Press, 1998, vol. 42, pp. 345.
28. Y. Iwata, Y. Araki, K. Honna, Y. Miki, K. Sato and H. Shimada, *Catal. Today*, 2001, **65**, 335.
29. T. Isoda, K. Kusakabe, S. Morooka and I. Mochida, *Energy Fuels*, 1998, **12**, 493.
30. H. Farag and I. Mochida, *J. Colloid Interface Sci.*, 2012, **372**, 121.

Catalysis Science & Technology Accepted Manuscript

31. C. Leyva, M. S. Rana, F. Trejo and J. Ancheyta, *Catal. Today*, 2009, **141**, 168.
32. A. S. Rocha, A. C. Faro Jr, L. Oliviero, J. Van Gestel and F. Maugé, *J. Catal.*, 2007, **252**, 321.
33. F. F. Ferreira, E. Granado, W. Carvalho Jr, S. W. Kycia, D. Bruno and R. Droppa Jr, *J. of Synchrotron Rad.*, 2006, **13**, 46.
34. M. Newville, *J. of Synchrotron Rad.*, 2001, **8**, 322.
35. A. L. Ankudinov, B. Ravel, J. J. Rehr and S. D. Conradson, *Phys. Rev. B: Condens. Matter*, 1998, **58**, 7565.
36. J. A. C. Faro, K. R. Souza, J. G. Eon, A. A. Leitao, A. B. Rocha and R. B. Capaz, *Phys. Chem. Chem. Phys.*, 2003, **5**, 3811.
37. E. P. Barrett, L. G. Joyner and P. P. Halenda, *J. Am. Chem. Soc.*, 1951, **73**, 373.
38. M. Egorova and R. Prins, *J. Catal.*, 2004, **225**, 417.
39. G. Smith, *Acta Crystallographica*, 1962, **15**, 1054.
40. D. Levin and J. Y. Ying, *J. Electroceram.*, 1999, **3**, 25.
41. K. Eda, Y. Kato, Y. Ohshiro, T. Sugitani and M. S. Whittingham, *J. Solid State Chem.*, 2010, **183**, 1334.
42. W. Xiao, J. S. Chen, C. M. Li, R. Xu and X. W. Lou, *Chem. Mater.*, 2009, **22**, 746.
43. L. M. Madeira, M. F. Portela and C. Mazzocchia, *Catal. Rev. Sci. Eng.*, 2004, **46**, 53.
44. K. S. Liang, R. R. Chianelli, F. Z. Chien and S. C. Moss, *J. Non-Cryst. Solids*, 1986, **79**, 251.
45. J. A. Rodriguez, S. Chaturvedi, J. C. Hanson and J. L. Brito, *J. Phys. Chem. B*, 1999, **103**, 770.
46. G. Berhault, M. Perez De la Rosa, A. Mehta, M. J. Yacaman and R. R. Chianelli, *Appl. Catal. A*, 2008, **345**, 80.
47. C. H. Wu, W. T. Reynolds Jr and M. Murayama, *Ultramicroscopy*, **112**, 10.
48. S. Eijsbouts, L. C. A. van den Oetelaar and R. R. van Puijenbroek, *J. Catal.*, 2005, **229**, 352.
49. A. Olivas, G. Alonso and S. Fuentes, *Top. Catal.*, 2006, **39**, 175.
50. H. Topsøe, R. Candia, N.-Y. Topsøe, B. S. Clausen and H. Topsøe, *Bull. Soc. Chim. Belg.*, 1984, **93**, 783.
51. T. Shido and R. Prins, *J. Phys. Chem. B*, 1998, **102**, 8426.
52. W. Wolfram Research Inc, *Mathematica*, Champaign, IL, 2010.
53. E. P. L. Hunter and S. G. Lias, *J. Phys. Chem. Ref. Data*, 1998, **27**, 413.
54. M. Villarroel, P. Baeza, N. Escalona, J. Ojeda, B. Delmon and F. J. Gil-Llambías, *Appl. Catal. A*, 2008, **345**, 152.
55. E. J. M. Hensen, P. J. Kooyman, Y. van der Meer, A. M. van der Kraan, V. H. J. de Beer, J. A. R. van Veen and R. A. van Santen, *J. Catal.*, 2001, **199**, 224.
56. S. Eijsbouts, J. J. L. Heinerman and H. J. W. Elzerman, *Appl. Catal. A*, 1993, **105**, 53.
57. M. Daage and R. R. Chianelli, *J. Catal.*, 1994, **149**, 414.
58. A. K. Tuxen, H. G. Füchtbauer, B. Temel, B. Hinnemann, H. Topsøe, K. G. Knudsen, F. Besenbacher and J. V. Lauritsen, *J. Catal.*, 2012, **295**, 146.
59. R. Koide, E. J. M. Hensen, J. F. Paul, S. Cristol, E. Payen, H. Nakamura and R. A. van Santen, *Catal. Today*, 2008, **130**, 178.
60. J. Shabtai, N. K. Nag and F. E. Massoth, *J. Catal.*, 1987, **104**, 413.

Catalysis Science & Technology Accepted Manuscript